CHAPTER V

REDUCING BACK RADIATION OF WRIST-WORN ANTENNA

5.1 INTRODUCTION

The heart of any wireless wearable system is an antenna, used as trans-receiving system, that is placed in proximity of a human body. Consequently, as the body is a lossy media the back radiations emanating from the antenna that enters the body dissipates as thermal energy and heats the adjoining tissues resulting in serious health risks [1]. In Chapter IV, it was observed, that presence of the human body influenced the electric field and surface current of the antenna. Moreover, the back lobe levels increased for the antenna on phantom as compared to free space, which might lead to increased penetration of fields inside the phantom. The current chapter proposes to reduce the extent of penetration of the back radiation using a dielectric lossy shield material based on expanded graphite.

Expanded graphite (EG) is a microwave absorbing material with low weight (density ~ 0.005–0.01 g/cc), high electrical conductivity of ~10^4 - 10^6 S/cm and is also resistant to environmental corrosion [2]. EG based dielectric composites have exhibited high dielectric loss $\varepsilon_r''/\varepsilon_r' > 1$ and a shielding effectiveness of ~ 45 dB [3]. EG sheets are also used as conducting layers to develop metamaterial inspired microwave absorber in the X-band frequency range [4]. If a thin sheet made up of expanded graphite be introduced between WBAN antenna and human body it may reduce the coupling of back radiation.

In the first phase of the current work the Topology I and II antenna (refer Chapter III) backed by a EG shield layer is designed and a full wave simulation is carried out using CST Microwave Studio to obtain the antenna parameters along with 2D electric field analysis. The six-layer numerical phantom developed in Chapter IV is used for the full wave simulation. The level of interaction of radiations with human interface is parameterized by Specific Absorption Rate (SAR) [5] and thus determined in the study. Post simulation a prototype is fabricated and evaluated for its reduction in back lobes employing the physical wrist phantoms synthesized in Chapter IV.

5.2 SYNTHESIS AND CHARACTERIZATION OF EXPANDED GRAPHITE (EG)

Expanded Graphite (EG) is synthesized from natural graphite flakes using the process of chemical oxidation and thermal treatment method [3]. Natural graphite flakes having size less than 2 μm is dried at 75°C for 8 hours to remove any moisture that may be present. The dried graphite flakes are then mixed with a saturated mixture of sulfuric and nitric acid in a volume ratio of 3:1. Sulfuric acid acts as the intercalant and nitric acid is the oxidizing agent. The graphite and acid mixture are kept for 12 hours and stirred continuously to get uniform intercalation. The chemically treated flakes are washed with distilled water to obtain a pH level of 7, and thereafter dried at 60°C. The dried flakes are exposed to high temperature of 800-900°C in a tubular muffle furnace to form expanded graphite.

X-ray diffraction of expanded graphite is conducted at room temperature with 2θ values from 10° to 70° using a Bruker AXS, Germany, Model - D8 Focus X-Ray Diffractometer, with a Cu Kα radiation of wavelength k = 1.541841 Å, as shown in Figure 5.1(a). The diffraction peaks centred at 2θ values of 26.56° and 54.60° correspond to (002) and (004) planes, confirming the formation of EG [3]. The inter-layer distance is calculated using Bragg's law and found to be 0.117 nm.

Scanning electron microscopy of the EG is carried out using a JEOL JSM 6390 LV model. SEM micrographs of EG at different scale are presented in Figure 5.1(c) and 5.1(d). Figure 5.1(c) with a scale of 100 μm shows vermicular or worm like structures, indicating the opening of a planar carbon network of natural graphite flakes. Figure 5.1(d) shows EG at lower scale of 10 μm, indicating that EG basically consists of numbers of graphite sheets [4].

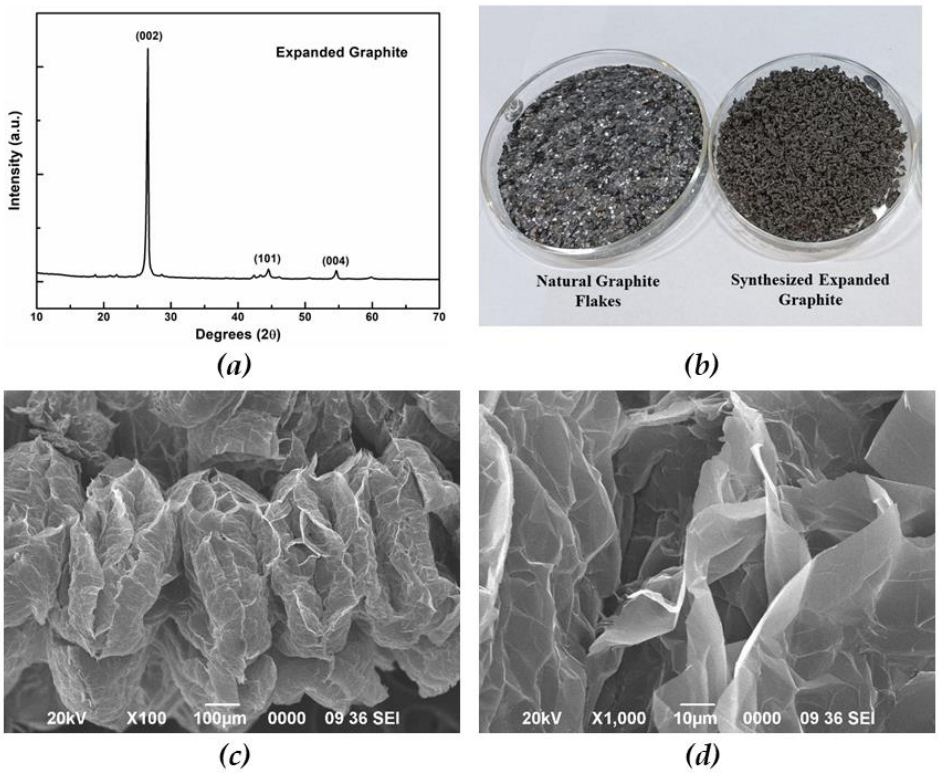

Figure 5.1 (a) X-ray diffraction pattern of expanded graphite, (b) natural graphite and synthesized expanded graphite, (c) SEM micrographs of expanded graphite at a magnification scale of 100 µm and (d) 10 µm

The laminated expanded graphite sheet is fabricated from the synthesized EG. The synthesized EG is grounded into powder form using a mechanical grinder (Retch ZM-200) and collected through a sieve of pore size 0.08 µm. The EG powder is spread uniformly over a microwave transparent adhesive tape and laminated by pressing (2 tons/cm^2) to obtain a flexible sheet of uniform thickness. Sheet of dimension (22.86 × 10.16 x 0.25) mm^3 of the laminated EG is cut out for carrying out microwave dielectric characterization in X-band as mentioned in Section 2.5 of Chapter II and illustrated in the inset of Figure 5.2(a).

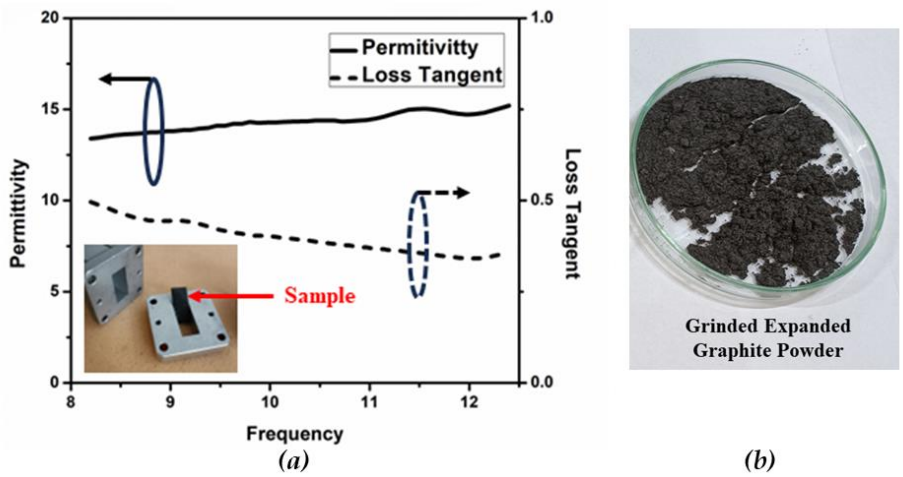

Figure 5.2 (a) Permittivity and loss tangent of expanded graphite sheet in X-band and (b) grinded form of expanded graphite

As seen from the dielectric spectra, the permittivity of the laminated EG sheet at 10 GHz is ~ 14 and the loss tangent is ~ 0.4.

The laminated sheet is also tested for its water absorbance and a weight change of ~0.001% is found after submerging the sample for 72 hours in water. The mass density of the sheet is measured to be 1.82 gm/cc.

5.3. DESIGN AND SIMULATION OF EG SHIELD

The laminated expanded graphite (EG) sheet is modelled in CST microwave studio importing the dielectric parameters as obtained in the preceding section. Essential requirement of the shield technique is to reduce the penetration of the back radiations into the human body and at the same time have minimal effect on the WBAN antenna performance. The EG prototype is proposed to be placed between the WBAN antenna and the human body thus acting as a shielding layer.

Thickness of the shield is optimized to obtain optimum reflectance and transmittance. Shield with thickness 0.5 mm, Figure 5.3(a) and 5.3(b), shows more than 25% reflectance in the working band indicating impedance mismatch and it will affect the antenna performance due to high back scattering. On the other hand, transmittance ~90% is observed for a thickness of 0.1 mm there is likelihood of coupling of the back radiation to the human body. Thus midway,

0.25 mm EG sheet can be considered as a trade-off in terms of both the reflectance and transmittance.

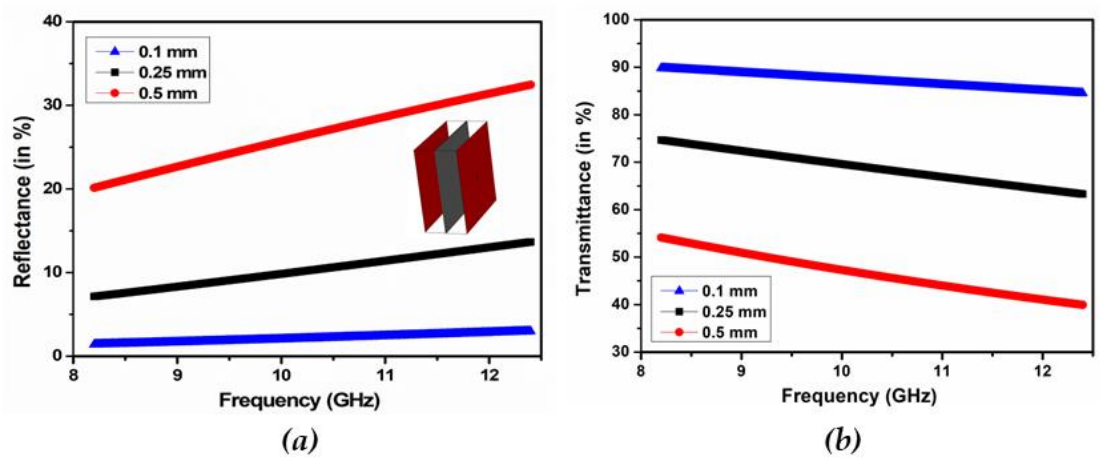

Figure 5.3 Simulated (a) reflectance and (b) transmittance of modelled laminated expanded graphite sheet of varying thickness in X-band regime

The shielding performance of the EG backed antenna is further optimized by the varying the gap between the ground plane of the antenna and the EG shield. A spacing or gap of 1 mm between in the EG shield and the antenna is found to reduce the back radiations further. The total thickness of the EG shield backed antenna is 3.25 mm as shown in Figure 5.4(a) and inset showing the individual layers with an expanded cross-sectional view. The EG shield backed antenna is placed in direct contact with the wrist phantom and the placement for Topology I and Topology II is illustrated in Figure 5.4(b) and 5.4(c) respectively.

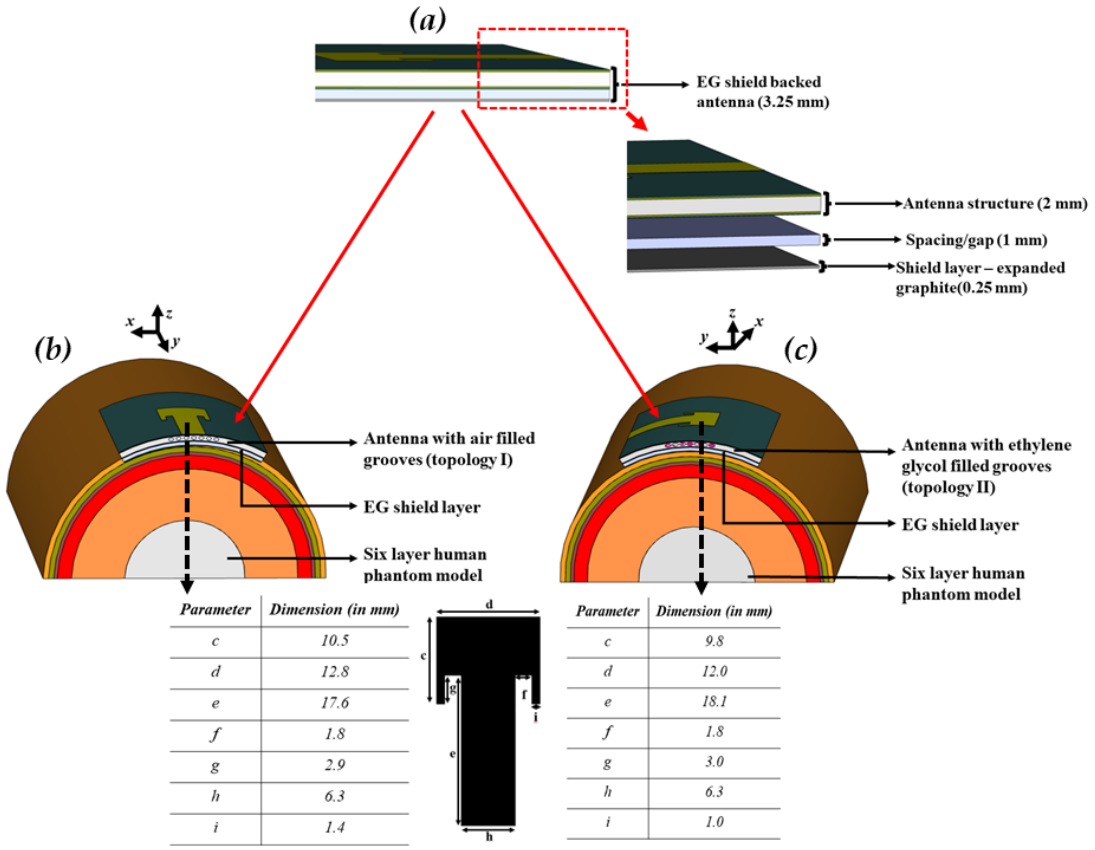

Parameter	Dimension (in mm)
c	10.5
d	12.8
e	17.6
f	1.8
g	2.9
h	6.3
i	1.4

Parameter	Dimension (in mm)
c	9.8
d	12.0
e	18.1
f	1.8
g	3.0
h	6.3
i	1.0

Figure 5.4 Schematic of (a) EG shield backed antenna (inset – individual layers of the antenna), (b) Topology I antenna and (c) Topology II antenna bent on a 40mm radius six-layer numerical human wrist phantom

Similar antenna without any EG backed layer and spacer but with an equivalent air gap thickness of 1.25mm (referred to as without EG in the following text) is also simulated to study the effect of the presence of the EG layer on the antenna's characteristics. The S_{11} characteristics of the Topology I antenna, both with and without EG layer, is plotted in Figure 5.5.

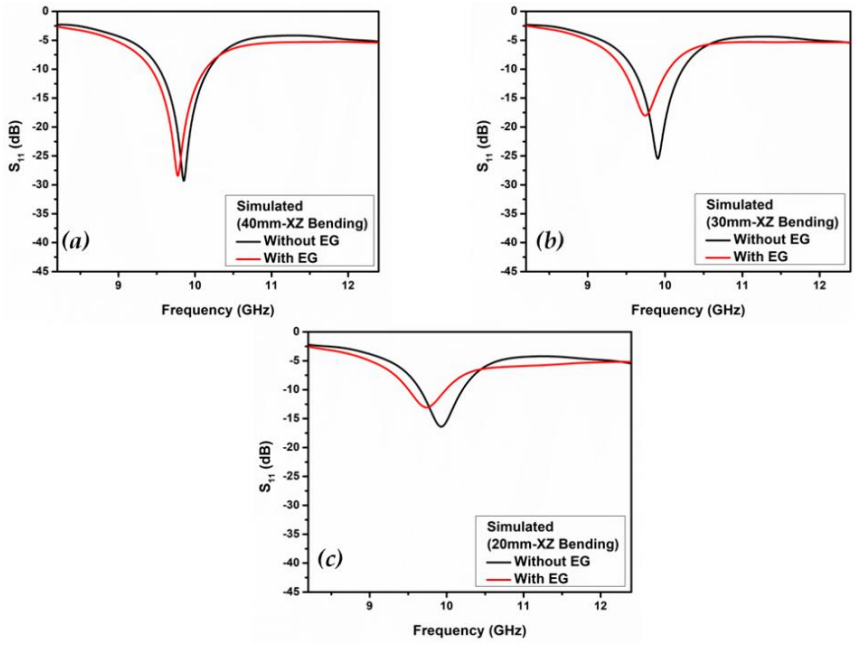

Figure 5.5 Simulated S_{11} plots (8.2-12.4 GHz) of Topology I antenna (black – without EG shield; red – with EG shield) bent along the XZ plane on wrist phantom of radii (a) 40 mm, (b) 30 mm and (c) 20 mm

The S_{11} plots of Topology II antenna system are shown in Figure 5.6.

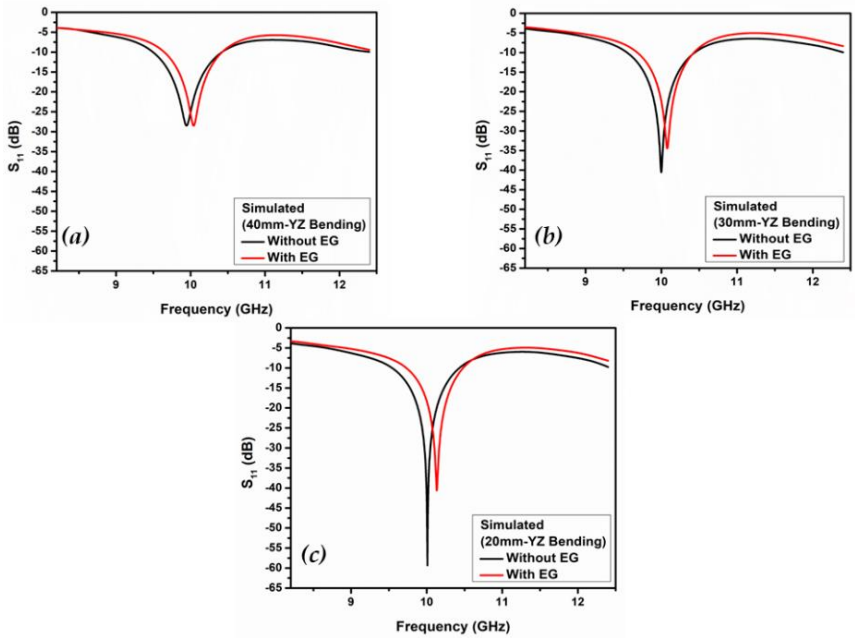

Figure 5.6 Simulated S_{11} plots (8.2-12.4 GHz) of Topology II antenna (black – without EG shield; red – with EG shield) bent along the YZ plane on wrist phantom of radii (a) 40 mm, (b) 30 mm and (c) 20 mm

The normalized XZ and YZ plane radiation pattern plots of the Topology I antenna are shown in Figure 5.7 and 5.8 respectively.

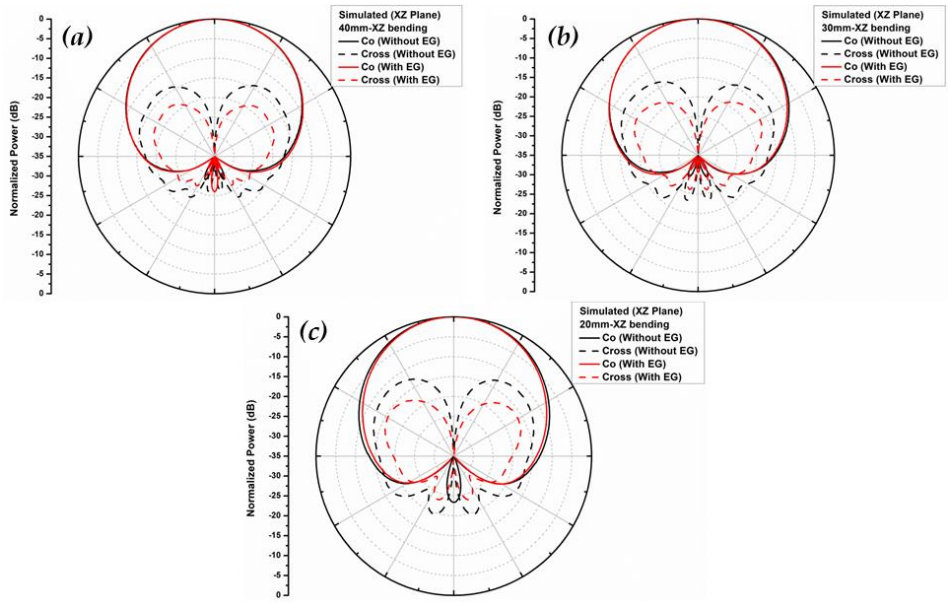

Figure 5.7 Simulated normalized XZ plane radiation pattern plots at the corresponding resonant frequency of Topology I antenna (black – without EG shield; red – with EG shield) bent along the XZ plane on wrist phantom of radii (a) 40 mm, (b) 30 mm and (c) 20 mm

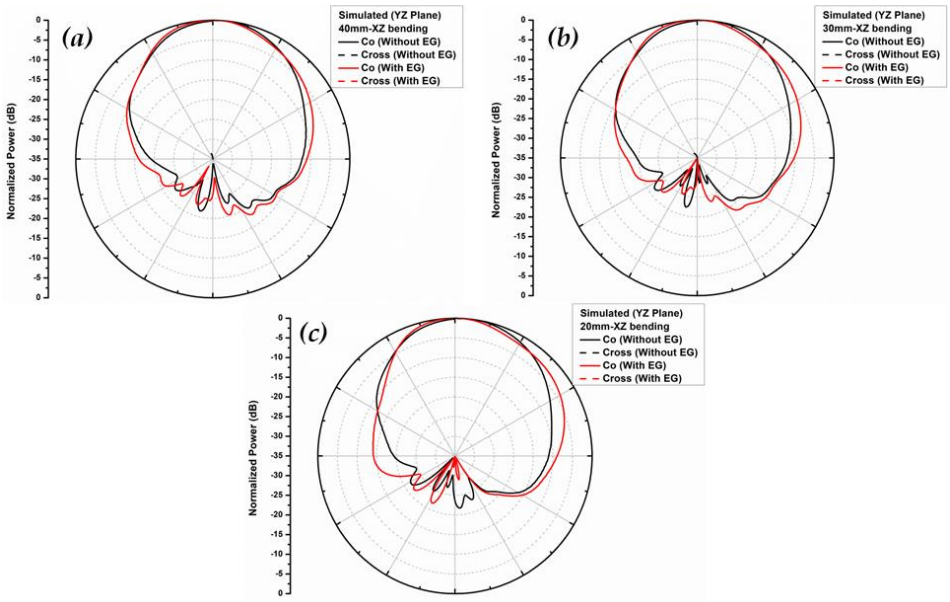

Figure 5.8 Simulated normalized YZ plane radiation pattern plots at the corresponding resonant frequency of Topology I antenna (black – without EG shield; red – with EG shield) bent along the XZ plane on wrist phantom of radii (a) 40 mm, (b) 30 mm and (c) 20 mm

The normalized XZ and YZ plane radiation pattern plots of the Topology II antenna are shown in Figure 5.9 and 5.10 respectively.

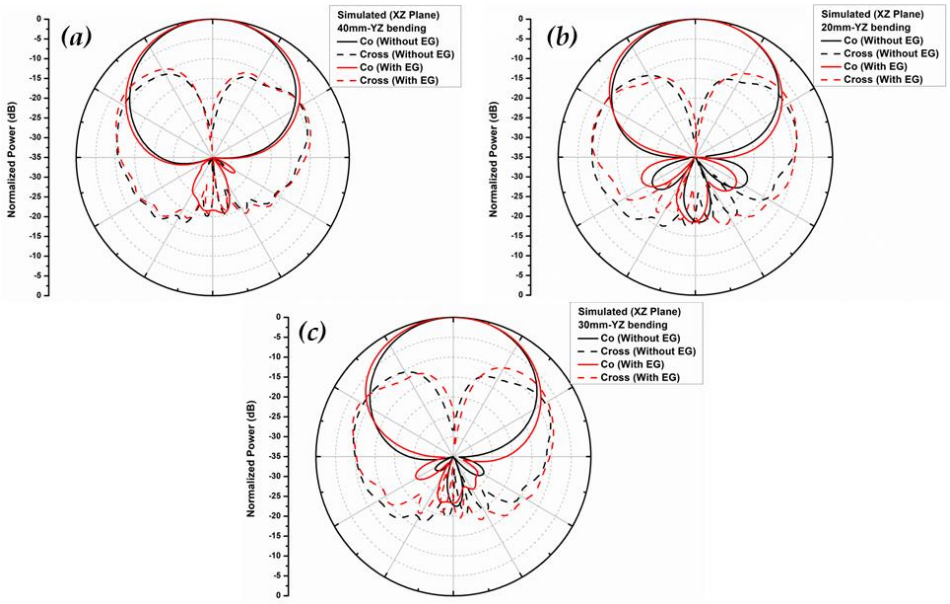

Figure 5.9 Simulated normalized XZ plane radiation pattern plots at the corresponding resonant frequency of Topology II antenna (black – without EG shield; red – with EG shield) bent along the YZ plane on wrist phantom of radii (a) 40 mm, (b) 30 mm and (c) 20 mm

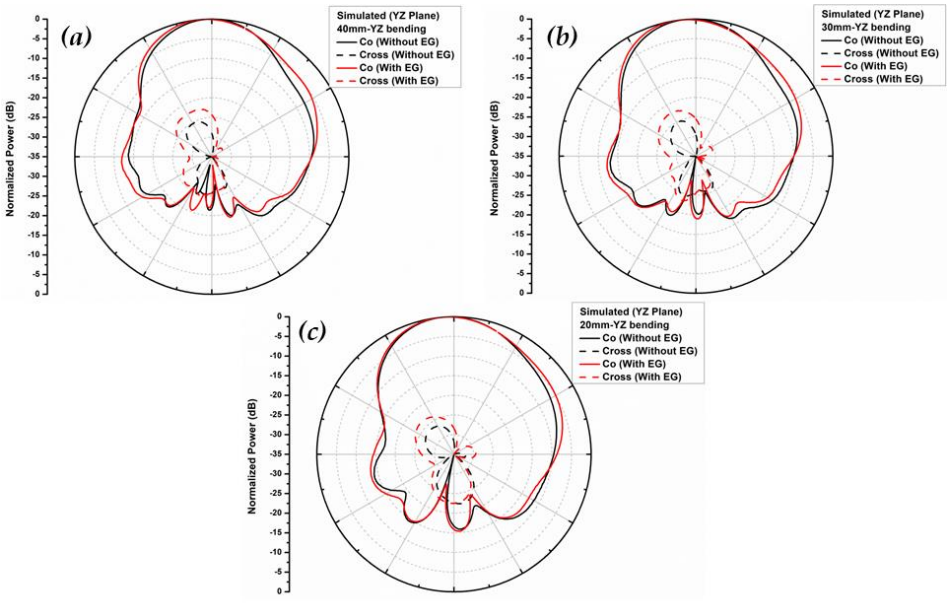

Figure 5.10 Simulated normalized YZ plane radiation pattern plots at the corresponding resonant frequency of Topology II antenna (black – without EG shield; red – with EG shield) bent along the YZ plane on wrist phantom of radii (a) 40 mm, (b) 30 mm and (c) 20 mm

The results of the simulation study are summarized in Table 5.1.

Table 5.1 Result summary of simulation study

Profile	*Bending Radii (mm)*	*Resonant Frequency (GHz)*	*S_{11} (dB)*	*-10 dB % BW*	*Directivity (dBi)*	*Gain (dBi)*	*Resonant Frequency (GHz)*	*S_{11} (dB)*	*-10 dB % BW*	*Directivity (dBi)*	*Gain (dBi)*
		With EG Shield					***Without EG Shield***				
Topology I	***40***	*9.77*	*-28*	*7.2*	*8.8*	*7.0*	*9.85*	*-29*	*6.5*	*8.8*	*7.0*
(XZ	***30***	*9.74*	*-18*	*6.0*	*9.1*	*7.5*	*9.90*	*-25*	*6.4*	*8.6*	*6.7*
Bending)	***20***	*9.73*	*-13*	*4.9*	*8.2*	*6.3*	*9.93*	*-16*	*5.4*	*8.2*	*6.1*
Topology II	***40***	*10.03*	*-28*	*7.6*	*8.6*	*7.0*	*9.94*	*-28*	*9.2*	*8.6*	*7.0*
(YZ	***30***	*10.07*	*-34*	*7.4*	*8.3*	*6.8*	*9.99*	*-40*	*8.9*	*8.3*	*6.7*
Bending)	***20***	*10.13*	*-40*	*7.3*	*8.0*	*6.5*	*10.01*	*-59*	*8.8*	*7.9*	*6.3*

EG shield has marginal effect on performance of the WBAN antenna. Though resonant frequency shows a slight shift, however the -10dB impedance bandwidth is almost consistent, with a trivial increase in gain and directivity for all the bending configurations.

5.3.1 Electric Field Analysis

An observation of the electric field along a plane cut parallelly with respect to the radiating edge of the antenna shall provide an insight to the effectiveness of the EG shield. Figure 5.11 and 5.12 are the electric field (maximum) 2D contour plots at the corresponding resonant frequencies of the Topology I and Topology II antenna respectively.

EG shield is found to suppress the electric field radiation underneath the whole dimension of the antenna for both the bending topologies which is erstwhile present in case of the antenna without the EG shield. However, there are fields that fringe around the edges of the antenna into the hand phantom.

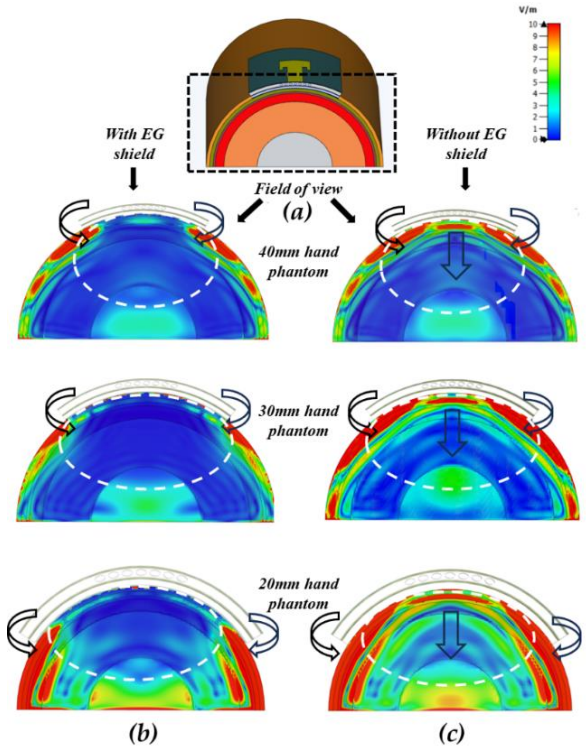

Figure 5.11 (a) Schematic of the field of view indicated by the dotted square for the 2D electric field pattern contour plots at the corresponding resonant frequency of Topology I antenna bent on 40mm, 30mm and 20mm wrist phantom, (b) with the EG shield and (c) without the EG shield

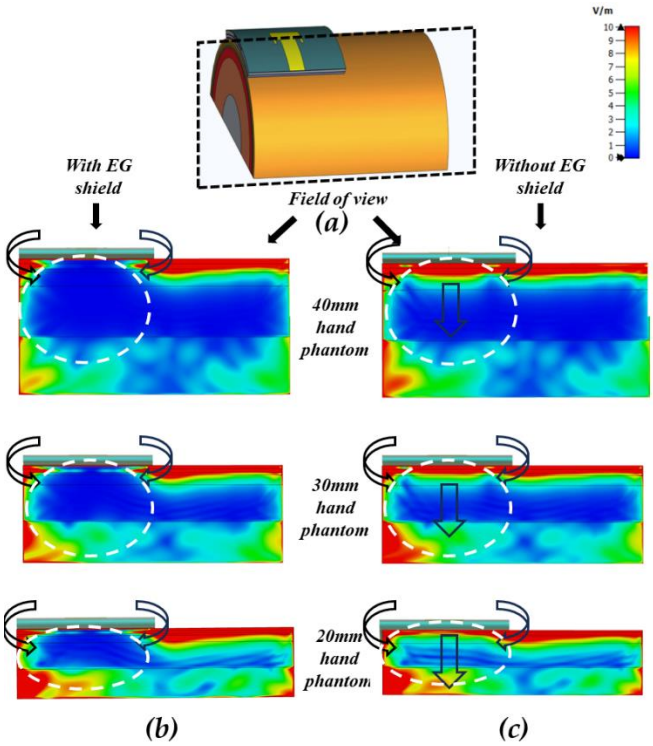

Figure 5.12 (a) Schematic of the field of view indicated by the dotted square for the 2D electric field pattern contour plots at the corresponding resonant frequency of Topology II antenna bent on 40mm, 30mm and 20mm radii wrist phantom, (b) with the EG shield and (c) without the EG shield

5.3.2 Specific Absorption Rate (SAR) Evaluation

The field absorbed by the tissue of the body field is responsible for the upsurge in the SAR values vide the relation (5.1) below

$$SAR = \int_{sample} \frac{\sigma(r)|\boldsymbol{E}(\boldsymbol{r})|^2}{\rho(r)} \qquad (5.1)$$

Where σ is the conductivity of the tissue and ρ is the mass density of the tissue. $\boldsymbol{E}$ is the electric field absorbed by the tissue and r is the position where $\boldsymbol{E}$ is measured.

A 2D plot of the SAR (10 gm average) of the Topology I and Topology II antennas are shown in figure 5.13 and 5.14 respectively. The peak SAR values are tabulated in Table 5.2. The input power of the feed had been set to 0.1 W which is the maximum allowed input peak power level for wearable devices [6].

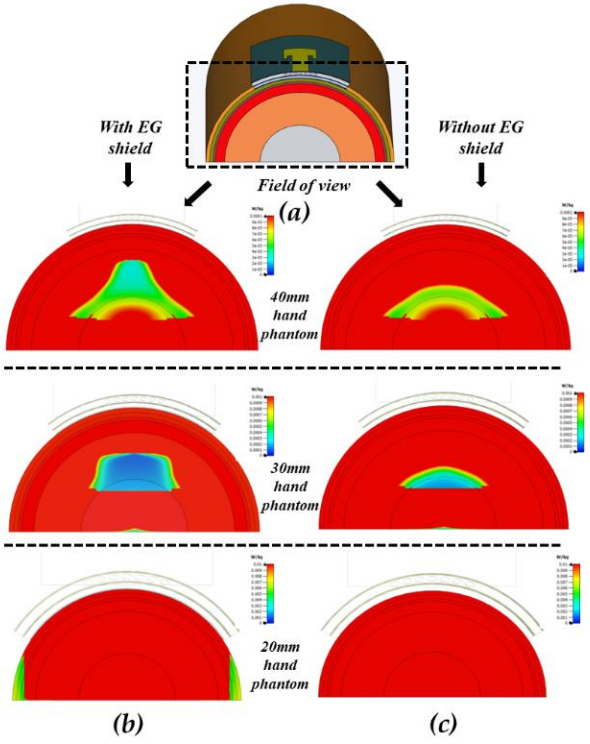

Figure 5.13 (a) Schematic of the field of view indicated by the dotted square for the 2D SAR pattern contour plots at the corresponding resonant frequency of Topology I antenna on wrist phantom of radii 40mm, 30mm and 20mm, (b) with EG shield and (c) without EG shield

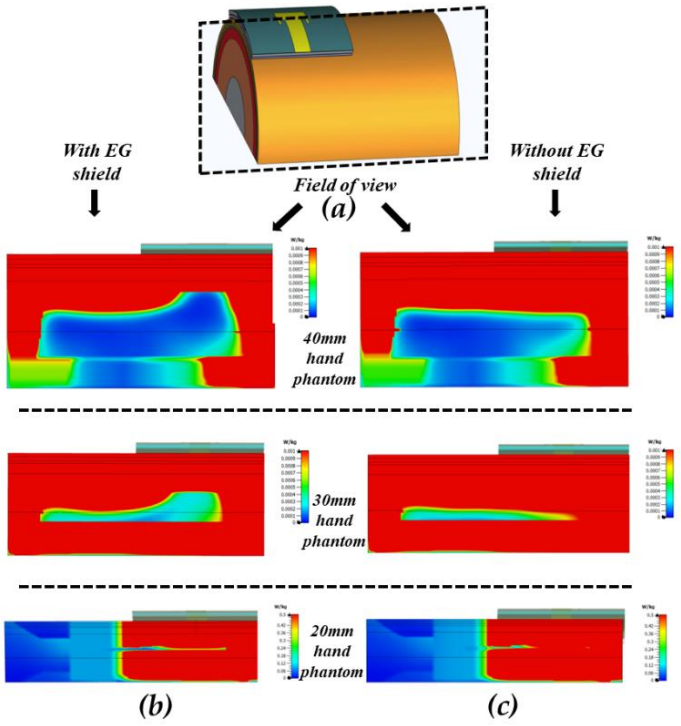

Figure 5.14 (a) Schematic of the field of view indicated by the dotted square for the 2D SAR pattern contour plots at the corresponding resonant frequency of Topology II antenna on wrist phantom of radii 40mm, 30mm and 20mm, (b) with EG shield and (c) without EG shield

EG backed antennas exhibit peak SAR values below the SAR limit as prescribed by ICNIRP, i.e., 4 W/kg for limbs averaged over 10 gm of the tissue (Table 5.2) [7]. A reduction of the peak SAR value of ~0.1 W/kg is seen for the antenna with EG as compared to without EG shield.

Table 5.2 Obtained Peak SAR values

Profile	*Bending Radii (mm)*	*Peak SAR (W/kg) – With EG*	*Peak SAR (W/kg) – Without EG*	*% reduction in SAR*
Topology I (XZ Bending)	***40***	*2.73*	*2.84*	*3.8*
	30	*2.39*	*2.51*	*4.1*
	20	*1.96*	*2.07*	*5.3*
Topology II (YZ Bending)	***40***	*2.6*	*2.63*	*1.1*
	30	*2.44*	*2.52*	*3.1*
	20	*2.72*	*2.84*	*4.2*

An increase in peak SAR values for YZ bending with decrease in bending radii is observed. In XZ bending the resonating length curvature does not change and the electric fields do not wrap around the phantom completely Figure 5.15(a). Whereas, in YZ bending the curvature of resonating length of the patch changes and the electric field on the surface of the antenna, refer Figure 5.15(b), encompasses around the phantom and consequently the fields penetrate till the core of the wrist.

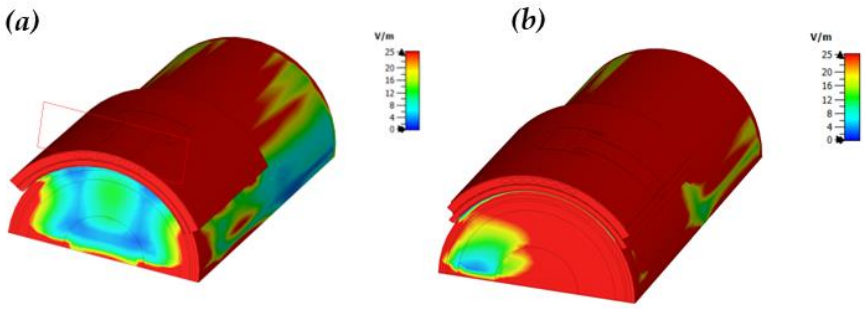

Figure 5.15 Electric field distribution of (a) Topology I and (b) Topology II antenna on 20mm radii wrist phantom

5.4 PROTOTYPING AND TESTING OF EG SHIELD WBAN ANTENNA

A laminated EG sheet of dimension 40 x 40 mm^2 is fabricated and attached to the bottom of the groove integrated antennas (both Topology I and II) using a microwave transparent double-sided adhesive tape (ε'~1.05 at 1-10 GHz) of thickness 1mm which also acts as the spacer for the EG backed antenna structure (Figure 5.16). Prior to attaching the EG shield the electrical continuity of the sheet is tested using a multimeter and found to be consistent across the edges of the shield. The measured thickness of the shield is found to be 0.26mm with an error bar of ±0.01 mm due to fabrication tolerances.

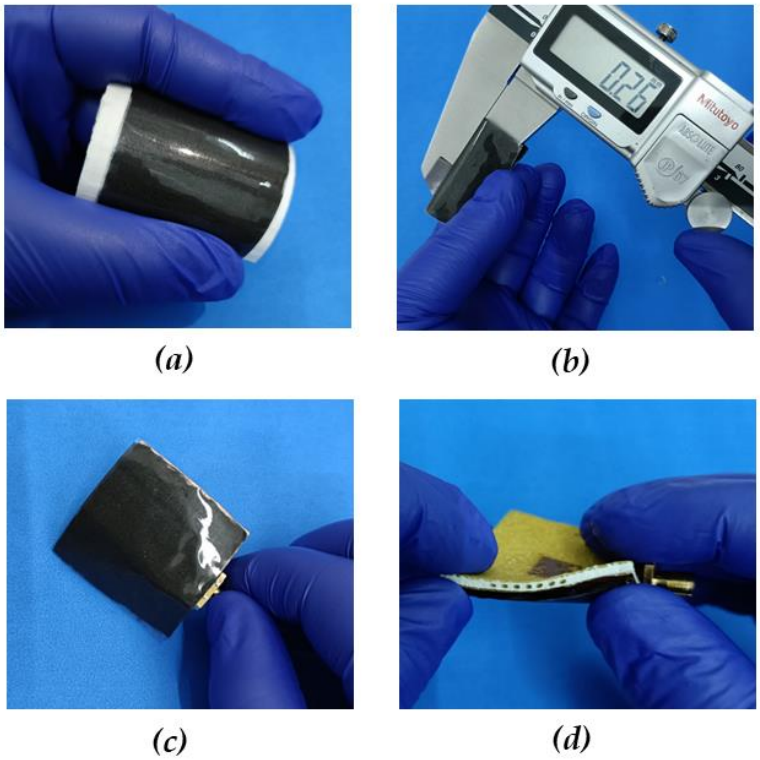

Figure 5.16 Photographs of the (a) fabricated laminated EG sheet, (b) EG sheet thickness, (c) EG shield attached to the bottom of the antenna and (d) EG shield backed Topology II antenna

The antennas are characterized for its resonating ability (S_{11}) and radiation capability as per the test set up mentioned in Section 2.6.1 in Chapter II. The radiation measurements are carried out along two orthogonal broadside planes. The antennas are tested by placing it over semi cylindrical graphite-based hand phantoms, developed in Chapter IV of radii 40 mm, 30mm and 20 mm.

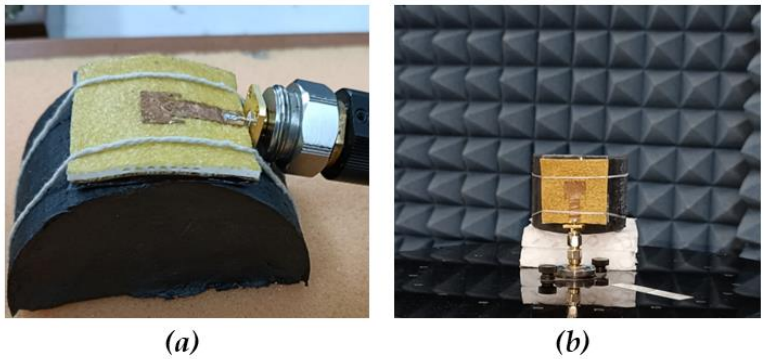

Figure 5.17 Photographs of the (a) Topology II antenna on 40mm wrist phantom connected to the VNA for S_{11} measurement and (b) Topology I antenna on 30mm wrist phantom placed on the turn table for radiation pattern measurement

The S_{11} curves of the Topology I and Topology II antenna with varying hand phantom radii are shown in Figures 5.18 and 5.19 respectively.

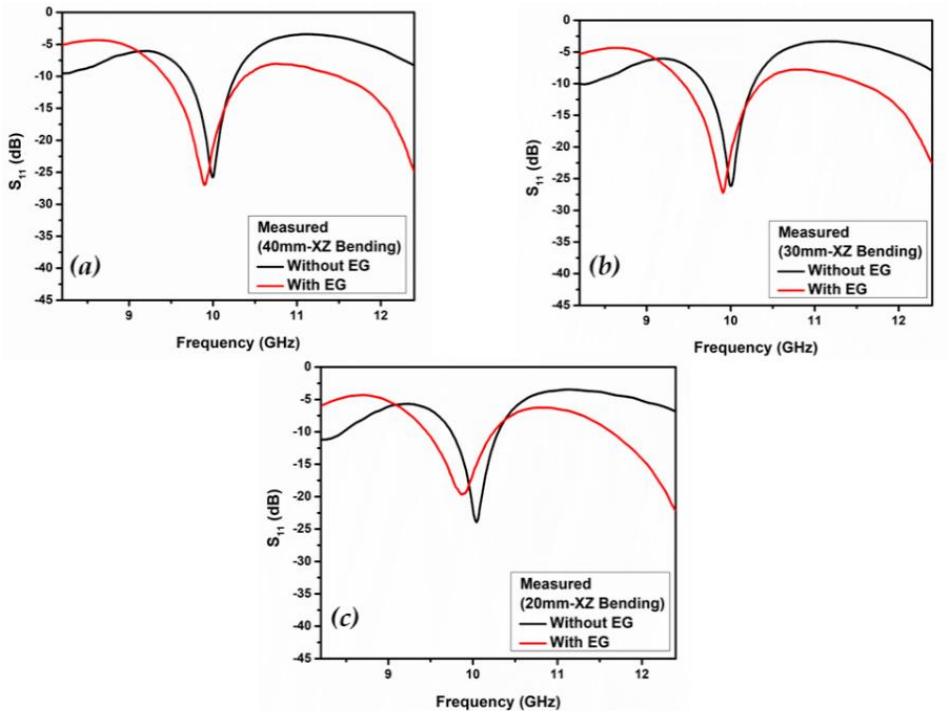

Figure 5.18 Measured S_{11} plots (8.2-12.4 GHz) of Topology I antenna (black – without EG shield; red – with EG shield) bent along the XZ plane on wrist phantom of radii (a) 40 mm, (b) 30 mm and (c) 20 mm

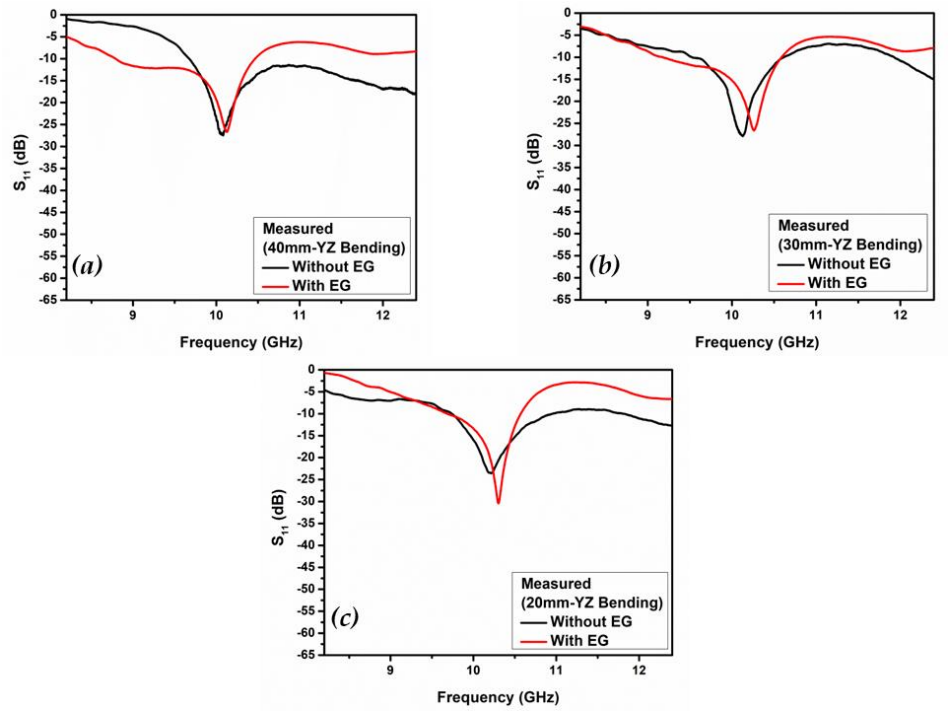

Figure 5.19 Measured S_{11} plots (8.2-12.4 GHz) of topology II antenna (black – without EG shield; red – with EG shield) bent along the YZ plane on wrist phantom of radii (a) 40 mm, (b) 30 mm and (c) 20 mm

The normalized XZ and YZ plane radiation pattern plots of the Topology I antenna are shown in Figure 5.20 and 5.21 respectively.

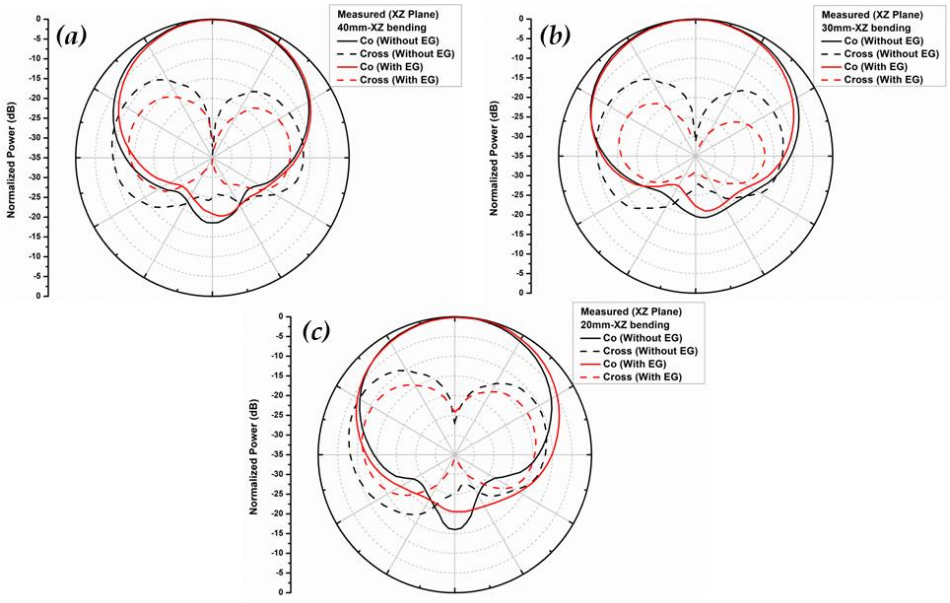

Figure 5.20 Measured normalized XZ plane radiation pattern plots at the corresponding resonant frequency of Topology I antenna (black – without EG shield; red – with EG shield) bent along the XZ plane on wrist phantom of radii (a) 40 mm, (b) 30 mm and (c) 20 mm

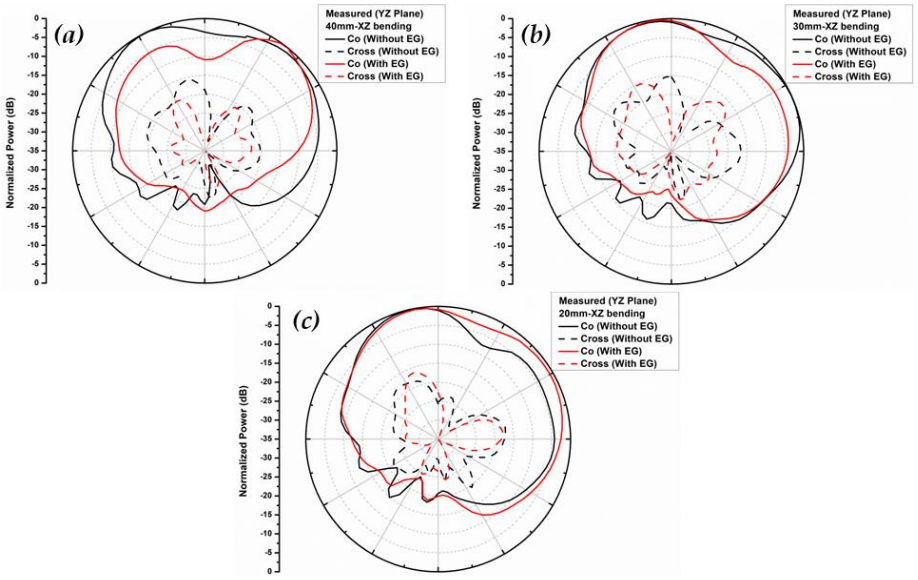

Figure 5.21 Measured normalized YZ plane radiation pattern plots at the corresponding resonant frequency of Topology I antenna (black – without EG shield; red – with EG shield) bent along the XZ plane on wrist phantom of radii (a) 40 mm, (b) 30 mm and (c) 20 mm

The normalized XZ and YZ plane radiation pattern plots of the Topology I antenna are shown in Figure 5.22 and 5.23 respectively.

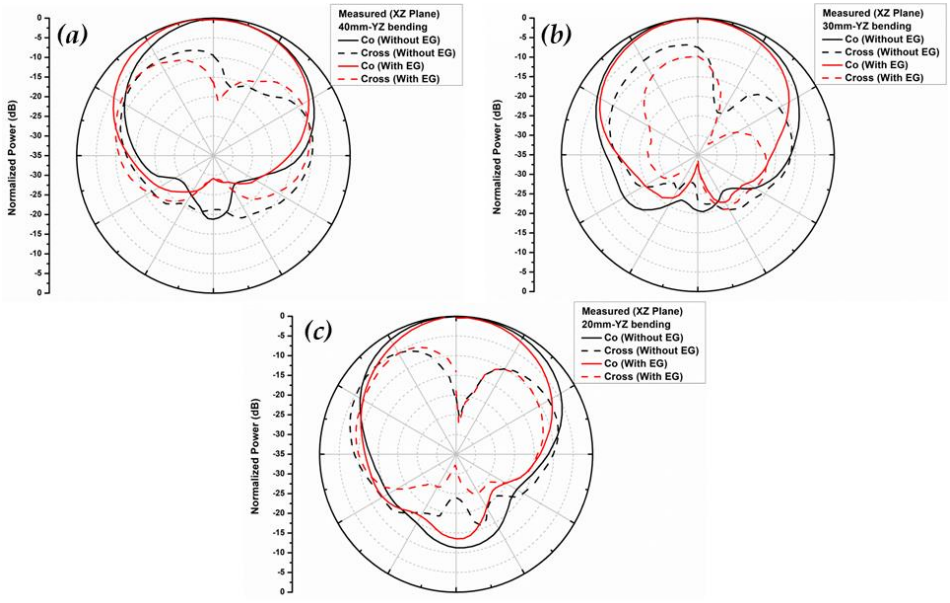

Figure 5.22 Measured normalized XZ plane radiation pattern plots at the corresponding resonant frequency of Topology II antenna (black – without EG shield; red – with EG shield) bent along the YZ plane on wrist phantom of radii (a) 40 mm, (b) 30 mm and (c) 20 mm

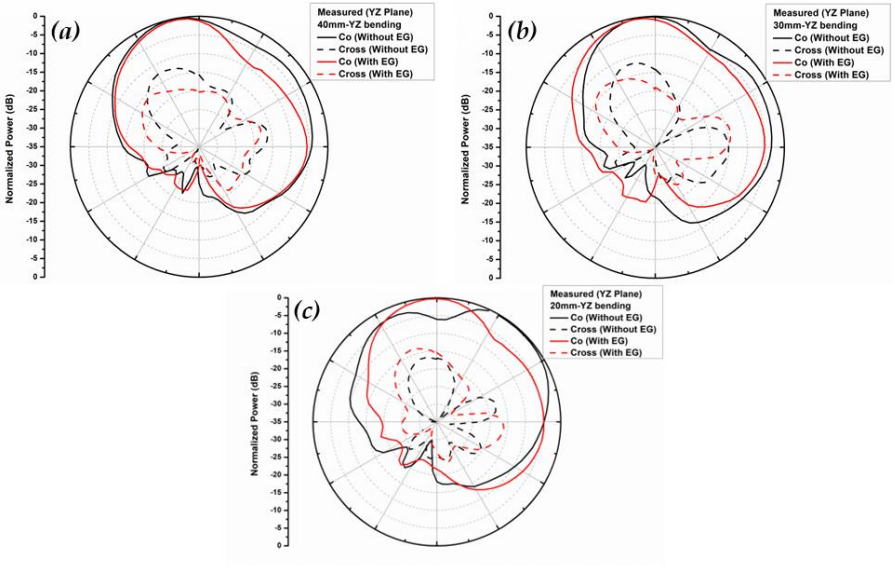

Figure 5.23 Measured normalized YZ plane radiation pattern plots at the corresponding resonant frequency of Topology II antenna (black – without EG shield; red – with EG shield) bent along the YZ plane on wrist phantom of radii (a) 40 mm, (b) 30 mm and (c) 20 mm

A summary of the experimental results has been tabulated in Table 5.3.

Table 5.3 Result summary of experimental study

Profile	*Bending Radii (mm)*	*Resonant Frequency (GHz)*	*S_{11} (dB)*	*-10 dB % BW*	*Directivity (dBi)*	*Gain (dBi)*	*Resonant Frequency (GHz)*	*S_{11} (dB)*	*-10 dB % BW*	*Directivity (dBi)*	*Gain (dBi)*
		With EG Shield					***Without EG Shield***				
Topology I (XZ Bending)	***40***	*9.89*	*-27*	*9.6*	*11.0*	*7.6*	*9.99*	*-25*	*5.8*	*10.4*	*7.2*
	30	*9.90*	*-27*	*9.4*	*10.0*	*7.4*	*10.00*	*-26*	*5.8*	*7.8*	*6.8*
	20	*9.86*	*-19*	*8.0*	*9.4*	*6.7*	*10.04*	*-23*	*5.5*	*8.3*	*6.0*
Topology II (YZ Bending)	***40***	*10.12*	*-26*	*16.5*	*11.1*	*7.1*	*10.08*	*-27*	*17.7*	*10.2*	*6.9*
	30	*10.26*	*-26*	*14.0*	*10.9*	*6.9*	*10.12*	*-27*	*10.7*	*9.7*	*6.7*
	20	*10.30*	*-30*	*8.6*	*10.9*	*6.8*	*10.21*	*-23*	*11.8*	*10.2*	*6.4*

The -10 dB impedance bandwidth enhances in presence of EG shield beneath the WBAN antenna. Interestingly, an enhancement of gain and directivity is also observed which may be due to the scattering of the back radiations towards the main lobe direction by the EG layer.

The trends followed by the measured and simulated results are similar, although slight differences are observed in the values, which might be because of the large computational structure of the phantom in addition to mesh cell restrictions of the simulation software leading to limitations in the actual electromagnetic representation of the modelled structures. Moreover, the difference in the composition of the phantom, six layer heterogenous in simulation and homogenous in measured, will naturally have distinct effects.

5.4.1 Back Radiation Reduction with EG Shield

A measure of the extent of back radiation of an antenna is estimated through the Front-to-Back Ratio (FBR) which is generally defined as ratio of the power radiated in the direction of the main lobe to the power radiated in the direction of the back lobe [8] and is expressed in dB.

$$FBR = \frac{Power\ radiated/received\ (main\ beam)}{Power\ radiated/received\ (180^{\circ}\ of\ the\ main\ beam)} \qquad (5.2)$$

A higher FBR indicates lower back lobes levels. The FBR of the antennas in the study are calculated from the experimental radiation patterns and are tabulated in Table 5.4.

Table 5.4 Obtained Front-to-Back Ratio values

Profile	*Bending Radii (mm)*	*FBR (dB) XZ plane*	*FBR (dB) YZ plane*	*FBR (dB) XZ plane*	*FBR (dB) YZ plane*	*Average % increase in FBR*
		With EG Shield		***Without EG Shield***		
Topology I (XZ Bending)	***40***	*26*	*26*	*13*	*20*	*65*
	30	*26*	*26*	*17*	*17*	*52*
	20	*22*	*22*	*12*	*13*	*76*
Topology II (YZ Bending)	***40***	*31*	*30*	*15*	*20*	*75*
	30	*30*	*29*	*19*	*20*	*51*
	20	*12*	*22*	*10*	*20*	*15*

EG backed WBAN antennas are found to have increased FBR, indicating the shielding which EG layer provides against the penetration of radiation into human phantom wrist. The higher FBR is also indicative of the subsided electric field values inside the wrist phantom and can thus be corelated to lower SAR as verified in the simulation studies.

The reflectance and transmittance of 0.25 mm thick EG shield is tested experimentally implementing the waveguide technique using VNA. The obtained curves are plotted in Figure 5.24. The reflectance and transmittance exhibited by the EG sheet is ~ 7% and 47% respectively.

The plots in Figure 5.24 are assertive of the nature of EG shield that have led to scattering and absorption of the radiation which otherwise would have penetrated the wrist phantom.

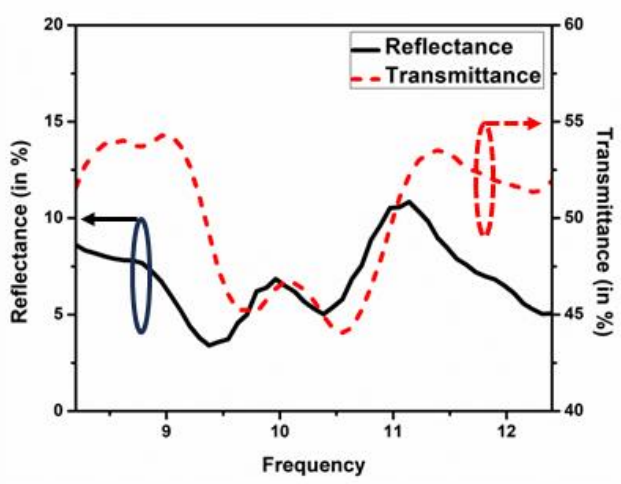

Figure 5.24 Reflectance and transmittance of fabricated 0.25 mm thick laminated expanded graphite sheet in X-band

5.5 SUMMARY

A flexible conducting lossy shield is developed and demonstrated for reduction in back radiation of linearly polarized X-band patch antenna for Wireless Body Area Network (WBAN) applications. The proposed structure comprises of a flexible patch antenna backed by a laminated sheet of Expanded Graphite (EG). The EG sheet is used as a protective shield to prevent back radiation emanating out of the WBAN antenna from propagating toward the human body. The antenna performance is tested over human wrist phantoms experimentally and through full wave simulation studies. The results indicate marginal variation in the -10 dB impedance bandwidth with slight increase in the gain and directivity values. A maximum measured on-body gain of 6.7 dBi is exhibited by the antenna backed by the EG shield. Electric field and SAR studies reveals reduction in wave penetration by the EG shield antenna inside the wrist phantom with a decrease of SAR by a maximum of 5%. Measured front-to-back ratio (FBR) values indicates lowering of back radiation with a maximum average increase by 76% exhibited by backed antenna which signifies the effectiveness of the EG shield employed in the study.

References

1. Ahmed, G., Islam, S.U., Shahid, M., Akhunzada, A., Jabbar, S., Khan, M.K., Riaz, M. and Han, K. Rigorous analysis and evaluation of specific absorption rate (SAR) for mobile multimedia healthcare. *IEEE Access*, 6:29602-29610, 2018.
2. Mahanta, U.J., Bhattacharyya, N.S., Hussain, I., Gogoi, P. and Gogoi, J.P. Design optimization and fabrication of a wideband microwave absorber based on dual-phase dielectric semi-metallic nanocomposite. *Journal of Physics and Chemistry of Solids*, 127:202-212, 2019.
3. Gogoi, J.P., Bhattacharyya, N.S. and Bhattacharyya, S. Single layer microwave absorber based on expanded graphite–novolac phenolic resin composite for X-band applications. *Composites Part B: Engineering*, 58:518-523, 2014.
4. Borah, D. and Bhattacharyya, N.S. Design and development of expanded graphite-based non-metallic and flexible metamaterial absorber for X-band applications. *Journal of Electronic Materials*, 46:226-232, 2017.
5. Lahiri, B.B., Ranoo, S. and Philip, J. Uncertainties in the estimation of specific absorption rate during radiofrequency alternating magnetic field induced non-adiabatic heating of ferrofluids. *Journal of Physics D: Applied Physics*, 50(45):455005, 2017.
6. Atanasov, N.T., Atanasova, G.L., Angelova, B., Paunov, M., Gurmanova, M. and Kouzmanova, M. Wearable antennas for sensor networks and IoT applications: Evaluation of SAR and biological effects. *Sensors*, 22(14):5139, 2022.
7. International Commission on Non-Ionizing Radiation Protection. Guidelines for limiting exposure to electromagnetic fields (100 kHz to 300 GHz). *Health physics*, 118(5):483-524, 2020.
8. Herscovici, N. A wide-band single-layer patch antenna. *IEEE Transactions on antennas and propagation*, 46(4):471-474, 1998.